Journal of Water Process Engineering 70 (2025) 106963

Contents lists available at ScienceDirect

Journal of Water Process Engineering

journal homepage: www.elsevier.com/locate/jwpe

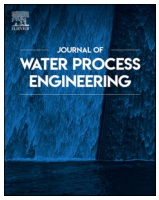

Understanding the difference between the nano and micro bubble size distributions generated by a regenerative turbine microbubble generator using ozone

Alexander John [a], Adam Brookes [b], Irene Carra [a], Bruce Jefferson [a,*], Peter Jarvis [a]

[a] Cranfield University, UK
[b] Anglian Water, Thorpe Wood House, Peterborough, UK

ARTICLE INFO

Editor: Laura Bulgariu

Keywords:
Microbubble
Nanobubble
Bubble size

ABSTRACT

There is a genuine paucity of data concerning the relative significance of the nano and the microbubble size distributions that are collectively generated when operating microbubble generation devices. Accordingly, the current work aimed to address this knowledge gap by measuring the two size distributions generated by a regenerative turbine microbubble generator using ozone and assess the relative significance of the nanobubble fraction. The microbubble fraction was measured with a focus-beam reflectance measurement device and the nanobubble fraction with a nano particle tracking instrument. The latter was calibrated using latex spheres to understand method uncertainty and to optimise the measurement approach. Sauter mean diameters of 217 nm and 37 μm were reported for the nano and microbubble fractions, respectively, with half of the microbubbles being <5000 nm in size. A comparison of the size and number concentrations of the different bubble types revealed that the majority of the gas was contained within the microbubble fraction, and hence, this controlled the overall mass transfer performance of the system. Further, the nanobubbles were observed to be stable for 18 h with little change in their size or number, indicating there was no net transfer of their gaseous contents. Overall, the work revealed that when considering enhancing gas-liquid mass transfer processes with micro-nano bubble generators, the microbubble fraction is key.

1. Introduction

The application of microbubbles in gas-liquid contacting processes has become established as a viable way to enhance performance in comparison to conventional bubble-liquid contactor systems [1,2,3,4,5]. Microbubbles are defined as bubbles with a diameter of 1–100 μm (ISO 20480-1:2017) and have a number of favourable properties compared with the larger bubbles formed in conventional gas liquid systems using porous diffusers, which are typically of a diameter of 2–6 mm [6,7,8,9]. The large difference in size between microbubbles and conventional bubbles means that microbubbles have a significantly lower buoyancy, lower rise velocity [10], and a much higher specific gas-to-liquid interfacial area [11]. As a result they have faster mass transfer [12] compared with conventional bubbles. For instance, in the case of ozonation used in drinking water treatment, using the same setup as reported in the current paper, the volumetric mass transfer coefficients (k_La) were 0.12 ± 0.004 for the conventional bubble and 0.30 ± 0.03 for the microbubble system operating at a pH of 6. Further investigation revealed that the mass transfer coefficient (k_L) was over 300 times lower for the microbubble system but that the mass transfer area was >500 times greater. The overall impact was an enhancement in mass transfer with the microbubbles by a factor of 2.5 [2,13]. Comparison of the ratio of reaction rate to mass transfer rate, through the Hatta number, revealed that the system was mass transfer dominated. As such, in situations where a reactant is being transferred from the gas to the liquid phase (for example, in ozonation and bioprocessing reactors), microbubble systems have been proven to be more effective [13], providing strong justification for their more widespread application.

In terms of ozonation reactors, this translates to higher dissolved ozone concentrations and, hence, more effective treatment when normalised to a fixed input ozone dose. To illustrate, in previous experiments by the current authors, comparative experiments at a fixed gas rate, with conventional and microbubble ozonation, resulted in steady-state dissolved ozone concentrations of 1.21 ± 0.03 mg/L for the

* Corresponding author.
E-mail address: b.jefferson@cranfield.ac.uk (B. Jefferson).

https://doi.org/10.1016/j.jwpe.2025.106963
Received 2 October 2024; Received in revised form 25 December 2024; Accepted 7 January 2025
Available online 9 January 2025

conventional bubble systems and 2.56 ± 0.07 mg/L for the microbubble system.

The generation of microbubbles from most devices usually results in the formation of both micro- and nanobubbles (MNBs). The latter have recently been identified as a route to potentially enhance mass transfer performance further. Nanobubbles are defined as bubbles with a diameter of 1–1000 nm, they have an extremely large specific surface area and are believed to have a high surface and internal energy for the facilitation of mass transfer [14,15]. Further, collapse of the nanobubbles has been associated with additional formation of free radicals and hence elevated reactions rates. Nanobubbles have also been reported to be extremely stable and long-lived in the order of weeks and months. The last two features are unique to nanobubbles and has generated significant interest for applications in agriculture [16], aquaculture [17], cleaning [18], environmental remediation [19] and water and wastewater treatment to remove micropollutants [20], enhance cleaning of reverse osmosis membranes [21], enhance oxygen transfer rates in wastewater treatment as well as offer an emerging option to replace existing microbubbles use in medicine for ultrasonic imaging and therapeutic purposes [22]. The function of the nanobubble is based on either enhanced mass transfer, prolonged transfer, scouring, negative zeta potential, or generation of a highly oxidative environment to aid reactions such as in the cleaning applications [23].

However, since the existence of nanobubbles was first proposed in 1981, significant debates remain about the existence of stable nanobubbles in the bulk solution since there is currently no definitive method to confirm whether observations are truly nanobubbles or other nano-entities such as particles or droplets [24]. Further, the established Epstein-Plesset theory on single-bubble lifetime predicts that bulk nanobubbles in gas-saturated liquids should remain stable for milliseconds [25]. The theory is based on the combination of the Young-Laplace equation, which describes how the pressure inside a bubble increases as the bubble size decreases, and Henry's law, which states that the solubility of a gas in a liquid is proportional to the pressure inside the bubble. Therefore, nanobubbles should be either inherently unstable or made unstable through natural perturbations [22]. Accordingly, a number of works have questioned the existence of nanobubbles [22,26,27,28,29,30,31] whilst numerous other works have reported their existence and long-term stability [32,33,34,35,36,37]. Nonetheless, the generation of nanobubbles has gained considerable interest with respect to gas-liquid contacting processes, and several works have reported nanometre-scale objects that they ascribe as bubbles (SI: Table S1). The importance of stability is positive to many bioprocessing and environmental applications [4,16,17,23]. However, in reactive ozone systems the persistence of nanobubble raising concerns downstream of the principal reactor where they are being generated.

The predominate difference between the two fractions is size. Microbubbles will be in the range 1–1000 μm and nanobubbles 1–1000 nm. Both enhance mass transfer compared to conventional bubbles (1–10 mm) and as such are becoming of interest to all applications that utilise bubble mass transfer. A key area for utilisation is bioprocessing applications where the ability to tune and maintain oxygen levels has been reported to be significant [23]. Examples include wastewater treatment with activated sludge, bio-production with yeast, algae, bacteria or plant-based systems. In all cases, application of either nanobubble or microbubble has seen enhanced growth compared to the control [23]. The additional properties of nanobubbles such as high zeta potentials, free radical generation and prolonged persistence have seen further benefits reported in terms of yield and selectivity within many bioprocessing applications [23]. The application is in its infancy but expected growth is reported to be substantial as the benefits become better understood and reported, especially in the bioprocessing field [23].

However, a knowledge gap exists concerning the relative significance that each fraction (micro- and nano-bubbles) provides in a co-generated system. This reflects unknown differences in both size and number to ascertain a total contribution. In part, this is driven by a lack of consistent reporting on bubble size distributions, especially when comparing MNB systems directly against conventional bubble systems [2]. In fact, to the best of the authors knowledge only one previous study has measured both micro and nano bubble fractions [42]. However, this study utilised a different generation system, was not based on ozone, used a small (1 L) vessel and did not compare the distributions in terms of the impact on potential reactions. The current work used a 100 L vessel to compare the performance of the combined MNB system with a conventional bubble system using ozone as a reactive gas for the degradation of pesticides. As both the nano bubble and microbubble fractions are co-produced it is not possible to independently assess the reaction performance of each fraction. Instead the current work utilises the size distributions to theoretically assess their relative contribution and the associated implications on future reactor configuration.

A number of different devices have been used to measure nanobubble size distributions including dynamic light scattering, nanoparticle tracking analysis and electrical zone sensing (SI: Table S1). The instruments work on a different fundamental principle from one another (light scattering, particle motion or electrical resistance) and require different background water characteristics. In the current work, the unknown nature of the distribution and the use of deionised water meant that the nanoparticle tracking instrument was the most appropriate. To better understand the uncertainty associated with the measurement, a series of calibration trials were conducted to ascertain the limits of the measurement and the uncertainty across a broad size range before measuring the nanobubbles.

Accordingly, the current paper aims to address the knowledge gap by directly measuring the micro and nanobubble size distributions produced from a regenerative turbine microbubble generator for bubbles containing ozone. NTA was used to measure the nanobubble fraction and focus-beam reflectance measurement was used for the microbubble fraction. Analysis of this novel data will provide a contribution to knowledge by establishing the relative contribution from each fraction. In addition, the work assesses the potential risk of stable ozone bulk nanobubbles progressing through a drinking water treatment works. The specific generator and application are selected as they represent an emerging potential market for the technology, and the corresponding performance data has already been reported [13]. Translation to alternative generators and applications is then discussed.

2. Materials and methods

2.1. Bubble generation

MNBs and conventional bubble measurements were conducted in semi-batch mode in 100 L of deionised water inside a cylindrical acrylic reactor with a height of 80 cm, a diameter of 45 cm and a water height of 62 cm (Fig. 1).

For the ozonation experiments, O_3 gas was generated from compressed air using a corona discharge ozone-generator (C-Lasky C-L010-DT, Advanced Ozone Products), with an operational gas flow rate of 2–10 L min^{-1}. The O_3 gas output of the generator was up to 2 g h^{-1} For all experiments, the gas flow rate of the ozone-generator was set to 2 L min^{-1}. For aeration experiments, ambient air was supplied to the microbubble generator through automatic suction.

MNBs were formed using a regenerative turbine microbubble generator (Nikuni KTM20N trial unit, Aeration & Mixing). The microbubble generator had a recirculating liquid flow rate of 16.6 L min^{-1} and a gas flow meter with a range of 0–5 L min^{-1}. The gas flow intake of the microbubble generator was set to 1–3 L min^{-1}, depending on the required gas flow rate. The aqueous phase was continuously recirculated through the microbubble generator. Conventional bubbles were generated from a fine pore diffuser (132 mm ceramic air stone diffuser, Finest Aquatic LTD) connected directly to the ozone-generator.

Fig. 1. Microbubble generation experimental apparatus.

2.2. Preparation of nanosphere calibration standards

The ability of the nanoparticle tracking analysis (NTA) system to detect and measure nano-sized entities was tested using calibration standards for a range of particle sizes and concentrations (example SEM images of the spheres can be found at reference [40]). Polystyrene-latex nanospheres of sizes 100 nm, 200 nm and 400 nm were tested (NTA4088, NTA4089, NTA4091, Malvern Instruments). The concentration of nanosphere preparations was calculated by the known parameters of particle diameter, density and percentage solids of the nanosphere. For each of the nanosphere sizes, suspensions of 1×10^7 # mL^{-1}, 1×10^8 # mL^{-1} and 1×10^9 # mL^{-1} were prepared according to the following equation:

$$c = 6{*}10^{10}\frac{W}{d^3\pi\rho} \tag{1}$$

Where c is particle concentration (# mL^{-1}), ρ is the density of nanospheres (kg m^{-3}), W is the percent solids of the nanosphere fraction and d is the nanosphere diameter (m). Blanks consisting of ultrapure water and water that had run through the microbubble generator without aeration were also analysed to determine whether contaminant nanoparticles were detectable.

2.3. Nanoparticle tracking analysis

The size distribution and number count of the nanobubbles were measured using a nanoparticle tracking instrument (Nanosight LM-20, Malvern Instruments). Dispersed objects were viewed as bright dots against a dark background, and video recorded utilising illumination with a 642 nm red laser delivered at 90° to the observation window. The video files were utilised to measure the mean square of the motion, which was then converted into a hydraulic radius according to the Stokes-Einstein equation:

$$D = \frac{(x,y)^2}{2t} \tag{2}$$

$$D = \frac{2k_BT}{3r_h\pi\eta} \tag{3}$$

Where D is the diffusion coefficient (m^2 s^{-1}), $(x,y)^2$ is the mean squared displacement of the particle (m^2 s^{-1}), t is time (s), k_B is the Boltzmann constant (J K^{-1}), T is temperature (K), r_h is hydrodynamic radius of the particle (m) and η is the dynamic viscosity of the liquid (kg m^{-1} s^{-1}).

For each sample, 5 mL was collected in a brand new 5 mL syringe. To load the sample, the sample chamber was removed and oriented sideways so that the sample chamber could be filled from bottom to top. The sample was added slowly so that the viewing pane was free from any voids. After measurement, the sample was removed using the syringe. Between runs, the sample chamber was flushed three times with ultrapure water followed by three rinses with the sample. The sample chamber was never dismantled for manual cleaning as it was easy to introduce contamination to the viewing window.

The method is known to be sensitive to the settings for recording and analysis and, in particular, the detection threshold in which the software excludes certain greyscale values from being tracked [38]. To determine optimal processing, each set of 10 captures was processed using 24 different detection thresholds from 2 to 50.

2.4. Microbubble and conventional bubble size distributions

The size distribution of the microbubbles was measured using a focus-beam reflectance measurement (FBRM) probe (600 L, Mettler Toledo). The probe was placed centrally in the bubble column and measured continuously over 30 min whilst the microbubble generator was running. The measurable range of the instrument was 1–4000 μm, and a minimum of 30,000 counts were collected per run. For the size distribution of the conventional bubbles, video was recorded using a waterproof high-speed camera (HERO8, GoPro). The camera was submerged in the water to avoid distortion from the cylindrical reactor. The camera was focused on a precision ruler with 1 mm spacing (Precision ruler, Dorcrafts), which acted as a size reference. The region was illuminated by a waterproof LED video light (XShot, Suptig), which was mounted to a camera tripod (JB01511-BWW, Joby). The video was shot

at 240 frames per second for 10 min. The video was slowed down to 30 frames per second and desaturated using video editing software (GoPro Studio, GoPro). Image frames from the video were extracted using media software (VLC Media Player, VLAN). The frames were processed manually using image processing software (ImageJ). The reference was measured in each frame, and in-focus bubbles were measured against it. A minimum of 1000 individual in-focus bubbles were measured for each run.

Once the distributions were collected, the Sauter mean diameter for the microbubble and conventional bubble distributions were calculated as follows [39]:

$$d_{32} = \frac{\sum n_i d_i^3}{\sum n_i d_i^2} \quad (4)$$

Where d_{32} is the Sauter mean diameter (m) and n_i is the number of bubbles with diameter d_i.

3. Results and discussion

3.1. Diameter measurement of polystyrene latex spheres

For each diameter and concentration combination, the measured diameter of the latex spheres appeared to increase as the processing detection threshold was increased. The variance in the measured diameter due to the different detection thresholds also increased as the particle number increased. For instance, with the 100 nm spheres, the difference between detection thresholds of 2 and 48 was 12.9 nm for a particle concentration of 1×10^7 # mL^{-1} increasing to 14.2 nm and 33.7 nm for particle concentrations of 1×10^8 # mL^{-1} and 1×10^9 # mL^{-1} respectively (Fig. 2). For the 200 nm spheres, the difference in measured diameter was 4.0 nm at a particle concentration of 1×10^7 # $mL^{-1,}$ which increased to 15.6 nm and 11.1 nm with particle concentrations of 1×10^8 # mL^{-1} and 1×10^9 # mL^{-1}. For the 400 nm spheres, the variance was much higher between the different detection thresholds. For example, at a particle concentration of 1×10^7 # mL^{-1}, the difference in measured diameter was 52.8 nm, while this increased to 69.3 nm and 102.8 nm for particle concentrations of 1×10^8 # mL^{-1} and 1×10^9 # mL^{-1}, respectively.

Taking an average value from multiple detection thresholds provides the benefit that it removes any influence of the operator. When the results from all detection thresholds were averaged, the measured diameters for the 100 nm spheres were 103.9 ± 3.7 nm, 106.8 ± 4.1 nm and 112.1 ± 11.0 nm at particle concentrations of 1×10^7 # mL^{-1}, 1×10^8 # mL^{-1} and 1×10^9 # mL^{-1}. For the 200 nm spheres, measured diameters of 208.0 ± 7.4 nm, 202.9 ± 4.9 nm and 185.5 ± 5.3 nm were found at particle concentrations of 1×10^7 # mL^{-1}, 1×10^8 # mL^{-1} and 1×10^9 # mL^{-1}. For the 400 nm spheres, measured diameters of 381.5 ± 12.7 nm, 368.9 ± 12.6 nm and 356.0 ± 24.1 nm were obtained for particle concentrations of 1×10^7 # mL^{-1}, 1×10^8 # mL^{-1} and 1×10^9 # mL^{-1}. Consequently, the measurement of nano-sized entities when using the nanoparticle tracker can be considered to be within approximately 10 % of the reported diameter (Fig. 2). These results are similar to previous work by Usfoor et al. [40], who found that larger diameter nanoparticles were consistently underestimated using this particle sizing method, and by Bachurski et al. [41], who noted that NTA overestimated diameter when measuring 100 nm spheres.

3.2. Concentration measurement of polystyrene latex spheres

Every concentration measurement varied by at least one order of magnitude across the full range of detection thresholds. To illustrate, when prepared to a concentration of 1×10^7 # mL^{-1}, the measured concentration for the 100 nm polystyrene latex spheres decreased from 1.08×10^8 # mL^{-1} at a detection threshold 2 to a value of 8.60×10^6 # mL^{-1} at a detection threshold of 48. Similar decreases in number count were observed for the calibration standards at prepared concentrations of 1×10^8 # $mL^{-1}$and 1×10^9 # mL^{-1} (Fig. 3). The same was true for the larger-sized calibration particles, although the level of variation appeared similar for all sizes. For example, in the case of the 400 nm particles, the measured concentration of the 1×10^7 # mL^{-1} standard was 1.73×10^8 # mL^{-1} at a detection threshold of 2 and 9.27×10^6 # mL^{-1} at a detection threshold of 48.

Despite the variation in measured concentrations, an optimal detection threshold was found for every combination of diameter and concentration (Supplementary Information [SI]: Table S2). The major problem with this, however, is that the optimal detection threshold was

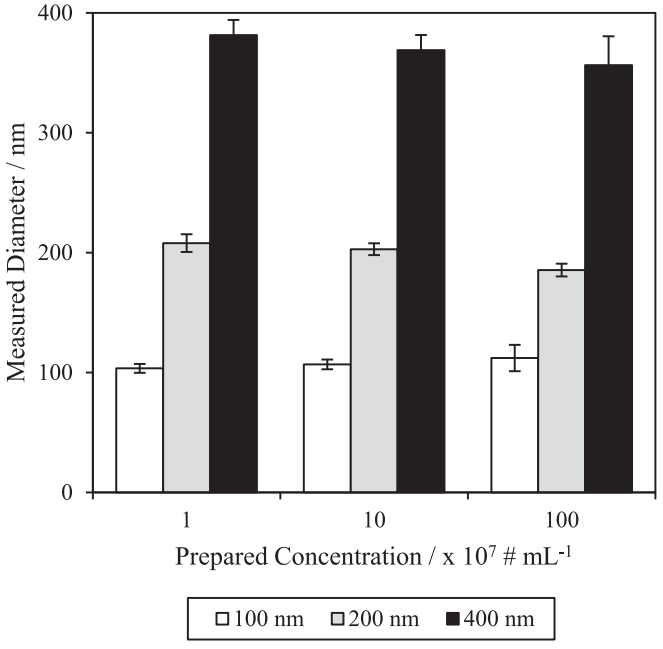

Fig. 2. Measured diameter (nm) vs. prepared particle concentration (x 10 ^{7} # mL^{-1}) for 100 nm, 200 nm and 400 nm polystyrene latex spheres.

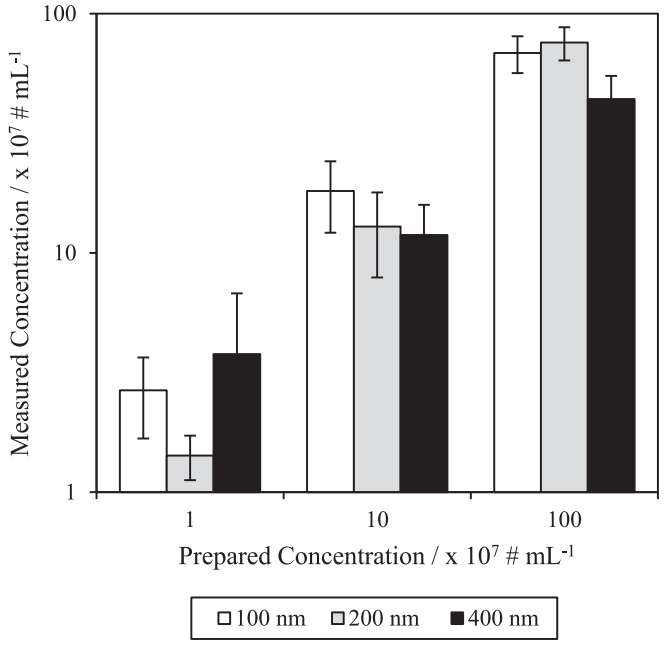

Fig. 3. Averaged measured concentrations across detection thresholds 2–50 for prepared concentrations of 1×10^7 # mL^{-1}, 1×10^8 # mL^{-1} and 1×10^9 # mL^{-1} for 100 nm, 200 nm and 400 nm polystyrene latex spheres.

different for every combination of diameter and concentration. Therefore, it would be virtually impossible to confidently measure the concentration of an unknown sample based on a single detection threshold. Further, there could easily be more than an order of magnitude of over- or under-measurement. The approach of averaging results across detection thresholds between 2 and 50 does not produce perfect concentration measurements However it attempts to reduce the variability that an operator could introduce into the results. To illustrate, for the 100 nm spheres at a prepared concentration of 1×10^7 # mL^{-1}, the measured concentration spanned across three orders of magnitude from 8.18×10^6 # mL^{-1} to 3.85×10^9 # mL^{-1}. By averaging across all detection thresholds, the measured concentration was $2.67 \times 10^7 \pm 4.24 \times 10^6$ # mL^{-1} which is much closer to the actual value.

In the current case, the average concentrations measured across all detection thresholds resulted for the 100 nm polystyrene latex spheres at prepared concentrations of 1×10^7# mL^{-1}, 1×10^8 # mL^{-1} and 1×10^9 # mL^{-1} were $2.67 \times 10^7 \pm 4.24 \times 10^6$ # mL^{-1}, $1.81 \times 10^8 \pm 9.00 \times 10^6$ # mL^{-1} and $6.84 \times 10^8 \pm 1.84 \times 10^7$ # mL^{-1}, respectively (Fig. 3). For the 200 nm spheres, measured concentrations of $1.42 \times 10^7 \pm 2.4 \times 10^6$ # mL^{-1}, $1.29 \times 10^8 \pm 1.06 \times 10^7$ # mL^{-1} and $7.57 \times 10^8 \pm 2.06 \times 10^7$ # mL^{-1} were found for prepared concentrations of 1×10^7 # mL^{-1}, 1×10^8 # mL^{-1} and 1×10^9 # mL^{-1}, respectively. Measured concentrations of $3.77 \times 10^7 \pm 6.44 \times 10^6$ # mL^{-1}, $1.19 \times 10^8 \pm 5.08 \times 10^6$ # mL^{-1} and $4.39 \times 10^8 \pm 9.06 \times 10^6$ # mL^{-1} were found for the 400 nm spheres at prepared concentrations of 1×10^7 # mL^{-1}, 1×10^8 # mL^{-1} and 1×10^9 # mL^{-1}, respectively. Overall, the measured number concentrations could be viewed to be accurate within one order of magnitude.

3.3. Size distributions of ozone MNBs

At gas flow rates of 1 L min^{-1}, 2 L min^{-1} and 3 L min^{-1}, the real-time size distribution of the ozone microbubbles was almost identical (Fig. 4). The vast majority of the size distribution was between 1 and 100 μm, with bubbles skewed towards the smaller sizes with 50 % being <5 μm. The Sauter mean diameter was 37 μm. This suggests that the regenerative turbine microbubble generator system produces a consistent size distribution irrespective of the gas flow rate. The mean diameters reported here are congruent with the work of Zhou et al. [42], who reported the majority of microbubbles formed with a fine bubble generator were <10 μm in size when measured using FBRM. Similar mean sizes between 1 and 10 μm have also been reported from both micro-nanobubble generators and high-speed rotation devices following measurement using a Coulter counter (SI: Table S1). The distributions were not normally distributed with a mode size of 3.7 μm, 3.8 μm and 3.5 μm at gas flow rates of 1 L min^{-1}, 2 L min^{-1} and 3 L min^{-1}, respectively (Fig. 4a). The corresponding number counts were 652 #, 696 # and 670 # respectively. This indicates the flowrate of the systems had minimal impact on either the size or the frequency of the measured microbubble distribution. When transformed into a cumulative distribution, the 25th, 50th and 75th percentiles bubble sizes were 3 μm, 4.6 μm and 9.9 μm respectively with a 1 μm variation in the upper percentiles as a function of flowrate (Fig. 4b).

The nanobubble fraction was measured by NTA with the sizes averaged across detection thresholds of 2–50 in order to remove any operator influence in the processing. The maximum detectable diameter with nanoparticle tracking analysis is 1000 nm, so it was assumed that micron-sized objects were excluded. The resulting size distribution was relatively uniform, with an average diameter of 217 ± 38 nm and 25th, 50th and 75th percentile diameters of 182 nm, 211 nm and 231 nm (Fig. 5). The breadth of the distribution was very narrow, with the majority of the bubbles sized below 130 nm. Comparison to other MNB generators and sizing instruments reveals a broad range of sizes reported, similar to those observed here (SI: Table S1). The average size measured in the current study was higher than those previously reported for bubbles generated by a range of methods, including a continuous high-shear rotor-stator device (similar to the one used in the current work), acoustic cavitation and water-ethanol mixing [32]. In these examples, NTA was used for bubble measurement with reported mean sizes between 95 nm and 125 nm, with the larger sizes being generated by the high-shear device. Interestingly, the bubble size data generated by the Coulter counter reported higher mean sizes, reflecting the difficulty in directly comparing data measured by different instruments.

The average concentration of nanobubbles across all capture conditions and detection thresholds was $2.9 \times 10^7 \pm 1.2 \times 10^7$ # mL^{-1} which was towards the high end of previously reported concentrations which varied between 1.84×10^5 # mL^{-1} and 7.5×10^8 # mL^{-1} (SI: Table S1). The previously reported work using a high shear device and nanoparticle tracking reported an initial bubble number density of 2.4×10^8 # mL^{-1}, albeit with a smaller mean diameter [32].

The nanoparticle tracking instrument does not differentiate between particles, droplets and bubbles, so it was not possible to confirm whether the measured distribution was nanobubbles. Indeed, the question as to whether the measured items are actually bubbles is an active area of debate, with compelling evidence for both positions. The source of potential nanoparticles when using devices such as the regenerative turbine microbubble generator includes contamination in the water, such as organics or inorganic particles, or from the release of metallic nanoparticles from the device. This has been confirmed in the case of ultrasonic cavitation, where titanium and vanadium nanoparticles were measured [22]. However, in other studies, no such organic or inorganic

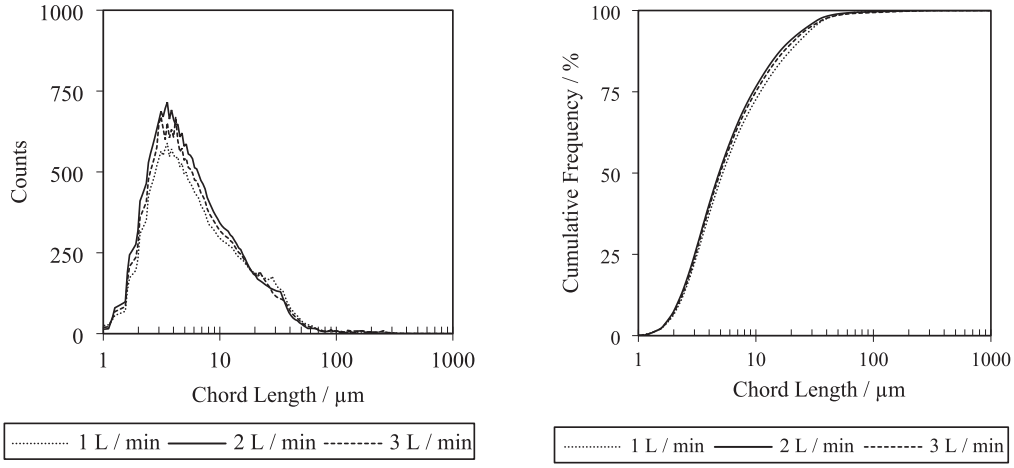

Fig. 4. Size distribution (left) and cumulative frequency (right) of microbubbles measured using focussed-beam reflectance measurement during ozonation at gas flow rates of 1, 2 and 3 L min^{-1}.

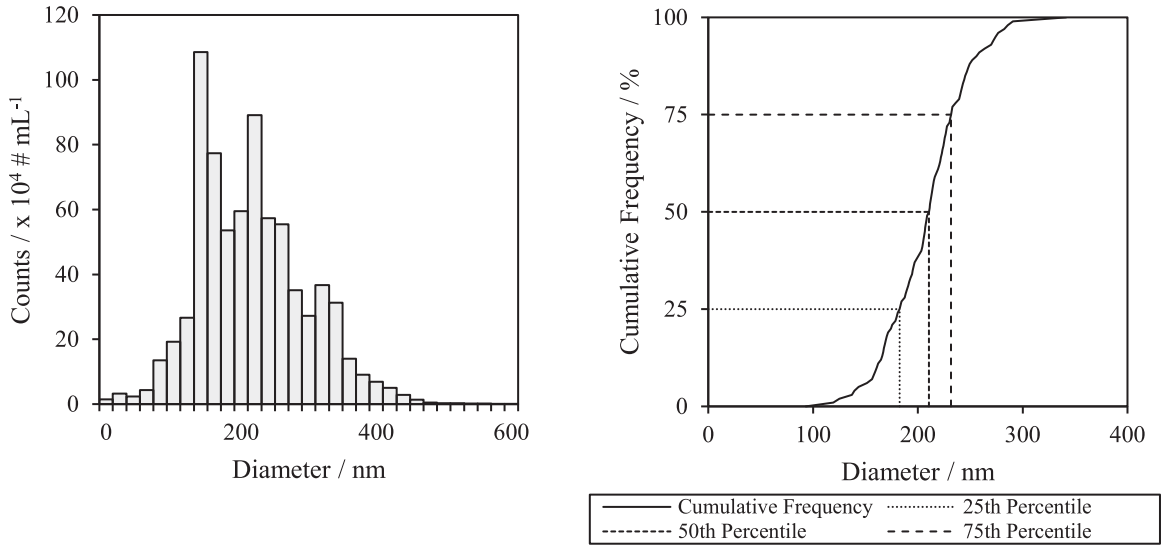

Fig. 5. Size distribution (left) and cumulative frequency (right) of residual ozone nanobubbles measured using nanoparticle tracking analysis with an original ozone gas flow rate of 2 L min^{-1}.

materials have been detected, and the amount of dissolved gas has a direct bearing on the number count while alteration in pressure impacts bubble size [32]. Interestingly, in the case of experiments using acoustic cavitation or water-ethanol mixing under a partial vacuum, an order of magnitude reduction in particle numbers was observed, which indicates that such entities must be gas-filled [32]. Overall, it remains unclear as to the exact nature of the nano-entities, but it is likely to be a combination of bubbles and non-bubbles (particles and droplets), the proportions of which will be system-dependent. In the case of the current trials, measurement of blanks and non-aerated water revealed that any other nanoparticles, if present, were sufficiently low in concentration to be below the limit of detection for the NTA ($< 10^6$ # mL^{-1}). This does not mean that nanoparticles were not present, but instead means that any detected particles, believed to be nanobubbles, were a result of the aeration process.

Direct comparison between the size distributions of the micro- and nanobubbles is complicated because they have been measured by different instruments. This means that the different distributions have different inherent biases, as well as differences in what is being measured (hydraulic diameter versus chord length). However, the distributions can be compared to explore the relative contribution both fractions will have in relation to mass transfer in gas-liquid systems, such as ozone contactors used in water treatment [43]. The microbubble fraction ranged between 1 μm and 100 μm with a mean diameter of 37 μm, while the nanobubble fraction ranged between 100 nm and 400 nm with a mean diameter of 217 nm. For context, the conventional bubble fraction ranged between 1 and 10 mm with a mean diameter of 5.4 mm [43]. The two systems can also be compared in terms of bubble volume and bubble number concentrations. In the case of the nanobubble fractions, the bubble number concentration is directly measured and was 2.9×10^7 # mL^{-1}. This equates to a bubble volume concentration of 0.715 mL m^{-3} based on a 217 nm bubble. The equivalent calculation of the microbubble fraction is based on the gas hold volume, which was measured to be 2.799×10^{-3} [13]. Accordingly, the bubble volume concentration is 2756 mL m^{-3} and the bubble number concentration is 2.56×10^6 number mL^{-1}.

The difference in size for micro- and nanobubbles was between 1 or 2 orders of magnitude, suggesting the differences in sizes were potentially less significant than previously thought for this type of MNB generator. Eklund et al. [38] illustrated the difference by comparing the properties of 100 nm (nano-) and 1000 nm (micro-) bubbles, i.e. the smaller end of each size range, at a typical nanobubble concentration of 10^8 # mL^{-1}. The bubble volume fraction relative to the liquid was 10^{-7} # mL^{-1} and 10^{-4} # mL^{-1} respectively, and so reasonably low in both cases. If no Laplace pressure in the bubbles is assumed, this then translates to gas concentrations of 0.0001 mg/L and 0.1 mg/L for the nano and micro scale bubbles, respectively. Adjusting to account for the Laplace pressure, assuming standard conditions would increase the concentration by an order of magnitude in the nanobubbles to 0.001 mg/L. This means that the majority of any transferred gas will still be associated with the microbubble fraction. In the current case, the gas transfer to the liquid is further weighted towards the microbubble fraction with, for instance, one individual 37 μm microbubble containing the same volume of gas as five million 217 nm nanobubbles. The smaller size of the nanobubbles will translate to a higher specific surface area, with values of 1.62×10^5 m^{-1} for the microbubble and 2.76×10^7 m^{-1} for the nanobubble in the current case. The specific surface area of the comparative conventional bubble system was 1111 m^{-1}. This should translate to a faster rate of mass transfer and, hence, enhanced performance as bubble size decreases. However, even for the microbubbles, the enhanced specific surface area compared to the conventional sized bubble system meant that almost complete gas transfer would occur within 1–2 m of water depth. To illustrate, a gas transfer efficiency of 96 % was reported in a 32 cm deep tank with microbubbles with a mean size of 51 μm [44]. In most water treatment applications, ozone tank depths exceed 3 m and can be as deep as 7–8 m [2]. Consequently, the benefits of enhanced mass transfer are realised with microbubbles and, indeed, could be larger than those currently considered. Further, the benefits of nanobubbles on enhanced mass transfer can only be realised in shallow tank depths and hence require new reactor designs to be developed. In addition, it has been proposed that for ozone systems MNBs can produce more hydroxyl radicals, enabling better and faster reactions. However, previous research has shown no statistically significant difference in radical formation when MNBs were compared to conventional bubbles (2–6 mm) when normalised for dissolved ozone concentration [43]. Previously reported enhancements are therefore driven by the increased mass transfer from the much higher specific surface areas associated with MNBs.

3.4. Longevity of residual nanobubbles

The other advantage stated for bulk nanobubbles is their stability over prolonged times. To test for the longevity of the residual nanobubbles from the current system. Samples were measured continuously

for 18 h using a custom script on the NTA system, which automatically captured the measurements every hour. Residual nanobubbles were detected consistently across the analysis period. The diameter of the residual nanobubbles immediately after the cessation of microbubble generation was 208.1 ± 24.9 nm, and the measured concentration was $7.17 \times 10^7 \pm 1.93 \times 10^7$ # mL^{-1}. Over the course of the 18 h, there was very little change in the measured diameter or concentration. The measured diameter did not appear to increase or decrease significantly and remained relatively static for the duration of the experiment at a size of 253 ± 61.4 nm (Fig. 6). The same was true for the measured concentration. After 18 h, there was a slight decrease in measured concentration to $2.09 \times 10^7 \pm 5.54 \times 10^6$ # mL^{-1}, although this was within the uncertainty range for the measurements (Fig. 7). Overall, this supports the idea of the longevity of nanobubbles, within the sensitivity limits of our measurements. Previously reported data from a similar system extended the trial to 140 days and showed that the number concentration decreased slightly over this time, but the size distribution decreased, with the majority of the bubbles being between 50 nm and 100 nm for the measurement taken after the first day [32]. In more recent work, the stability of carbon dioxide (CO_2) nanobubbles has been reported to be associated with pH [45]. Specifically, in their experiments at pH 4, the CO_2 was in a supersaturated state making it difficult for further dissolution.

While the stability of bulk nanoparticles remains an open area of debate, a number of theories have been proposed to help explain the deviation from the established Epstein-Plesset theory. The established position suggests nanobubbles in saturated liquids should be stable for no more than a few milliseconds [22]. The alternative theories include the skin model and the armoured bubble model, where surfactant and organic layers on the outside of bubbles stabilise them; the electrostatic repulsion model related to the very high magnitude zeta potential that nanobubbles are reported to have; and a dynamic equilibrium model [46]. Surface coating in real waters is likely, but the exact extent and type will vary. Such surface accumulation can reduce the surface tension and, hence, the Laplace pressure such that the bubble can exist in equilibrium with the surrounding saturated liquid. Similarly, the dynamic equilibrium model proposes patchwork hydrophobic zones on the bubbles that aid diffusion into the bubble, whereas gas can diffuse out

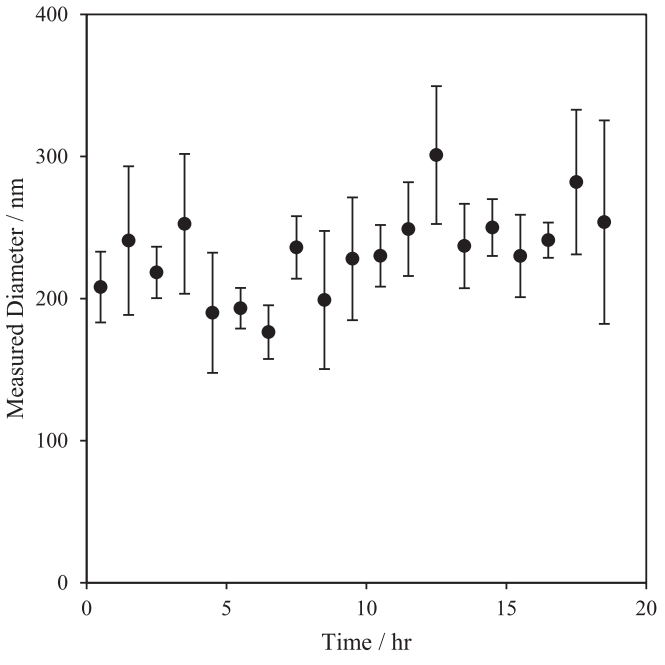

Fig. 6. The measured diameter of nanobubbles over an 18-h time period from the point of generation. Bubbles were produced using a regenerative turbine pump and air as the filling gas.

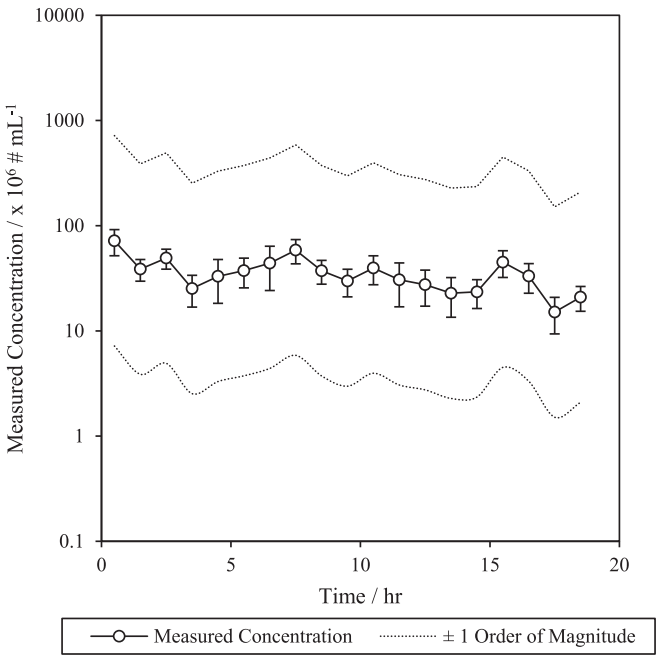

Fig. 7. The measured concentration of nanobubbles over an 18-h time period from the point of generation. The dashed line above and below the observed concentrations shows the order of magnitude difference in concentration to demonstrate that any change is within the uncertainty bands of the measurement. Bubbles were produced using a regenerative turbine pump and air as the filling gas.

into the liquid through the uncovered areas. The net is no overall transfer, and hence, the bubbles are stable [47]. No one model currently explains the phenomena observed, and there is often limited direct evidence such that no common theory currently exists [46]. However, one important aspect is common to a number of these ideas: there is no net gas transfer, and hence, the nanobubbles are unlikely to contribute to overall transfer and performance enhancement. If the stable size is due to gas transfer equally in both directions, the new gas will be inert and hence no long-term contribution can be expected.

Overall, the work indicates that, nanobubbles are unlikely to be the key component that delivers enhancement in gas-liquid treatment systems used in water treatment. Instead, and particularly in the case of ozone, the fate of the nanobubbles represents a potential concern as they will likely exit the ozone contactor into the downstream processes. Residual dissolved ozone is typically removed by adsorption onto granular activated carbon (GAC) beds that are positioned after the ozone contactors, Thus ensures no residual carryover of ozone in the later stages of treatment to minimise potential ozone off-gassing post-contactors (release of ozone into the atmosphere) [48]. However, the fate of stabilised nanobubbles is unknown and represents an area of urgent need for investigation. Nanoparticles of around 100–200 nm are normally relatively easily removed in depth filter operations and GAC beds as they will have a very high collision efficiency, which means that they will contact the media. However, the likely surface coating and the high negative zeta potentials associated with nanobubbles means that they are expected to have a very low attachment efficiency [49]. Hence nanobubbles could pass through these post-ozone stages. Calculation of the maximum potential impact based on our current data of a mean nanobubble diameter of 217 nm and a bubble concentration of 2.89×10^7 # mL^{-1} translates into a potential quantity of molecular ozone of 0.32 μg L^{-1}. Factoring in the observed uncertainty presented, an ozone concentration range between 0.032 and 3.2 μg L^{-1} may be possible. In addition, ozone generators do not produce 100 % ozone gas. A typical ozone output for a pure oxygen feed gas is 6–13 % [50] and is significantly lower for air-fed systems. Therefore, the potential quantity of

molecular ozone within nanobubbles is likely to be much lower than stated. Current legislation for ozonation is focused on the formation of bromate from the ozonation of bromide in bromide-containing waters. Bromate is a potential human carcinogen with a regulatory limit of 10 μg L^{-1} [51]. Undissolved and unquenched gaseous ozone passing through to post-ozone stages risks the formation of additional bromate. However, the gaseous ozone volume entrained within the nanobubbles is thought to be sufficiently low so as not to be a cause for concern.

Translating the findings to other generator systems should yield similar outcomes, given that the reported sizes from other devices are within the same range as reported in the current case (SI: Table S1). Application of any of these devices for other gas-liquid mass transfer applications such as bioprocessing, will yield the same finding, in that optimisation of mass transfer should focus on the microbubble fraction. Further, sensitivity to bubble size within the microbubble fraction will be limited when used in traditional reactors as (near) complete gas transfer will occur within less than half of the available water depth [2]. Translation to applications where the nanobubble fraction is ascribed more prominence, such as in membrane cleaning [25,52], places more emphasis on developing higher nanobubble concentrations. There is known to be more difference between different generation devices enabling a basis for technology selection (SI: Table S1). Overall, there is an urgent need to establish the optimum bubble size(s) required for different applications so that the benefits of micro-nano bubble generation can be fully realised. In addition, empirical verification of the relative contribution is needed. This requires a method to separately generate the two bubble fractions to enable controlled experiments and is an area for future work.

4. Conclusion

The work has independently measured the nanobubble and microbubble size distributions coproduced using a regenerative turbine microbubble generator with ozone. The microbubble fractions were measured using FBRM and the nanobubble fraction measured using nanoparticle tracking. The latter was calibrated using latex spheres and identified an uncertainty level of around 10 % on the size measurements.

Mean bubble sizes of 217 nm and 37 μm were reported for the nanobubble and microbubble fractions, respectively, both with reasonably distributed size ranges. Further, 50 % of the microbubbles were <5000 nm in size, such that the two distributions differed by around one to two orders of magnitude in size. Interpretation of the findings, with regards to water treatment using an ozone gas-liquid contactor, indicated that the nanobubble fraction is unlikely to be a significant contributor to the efficiency and effectiveness of the process and that the majority of the performance is delivered through the microbubble fraction. Estimation of the gas contained per bubble in each fraction, accounting for enhanced gas content due to the Laplace pressure in the nanobubble, indicated resultant ozone concentrations of 0.001 and 0.1 mg/L. This suggests that more focus should be placed on understanding how to control the size distribution of the microbubble fraction in order to optimise the overall process. Such findings translate to all other gas-liquid mass transfer systems. Where the water depth is above a couple of metres, the benefits will be realisable for bubbles produced from all of the available MNB generator technologies.

The nanobubbles were observed to remain stable in terms of number and size for 18 h. This further supports the negligible impact of the nanobubble fraction on mass transfer but raises concerns as to their fate as they are likely to exit the contactors. Based on the measured data, the risk for residual ozone through nanobubble survival was considered negligible, with an estimated maximum ozone residual of 3.2 μg L^{-1} predicted under typical water treatment conditions. However, work is required to confirm the fate of nanobubbles through downstream processes such as GAC. The potential future outlook for using micro-nano bubble systems is good, but a clear understanding of the optimum bubble size for different applications is needed.

CRediT authorship contribution statement

Alexander John: Writing – original draft, Methodology, Formal analysis, Data curation. **Adam Brookes:** Writing – review & editing, Supervision. **Irene Carra:** Writing – review & editing, Supervision, Methodology, Funding acquisition, Conceptualization. **Bruce Jefferson:** Writing – review & editing, Supervision, Funding acquisition, Conceptualization. **Peter Jarvis:** Writing – review & editing, Supervision, Funding acquisition, Conceptualization.

Declaration of competing interest

The authors declare that they have no known competing financial interests or personal relationships that could have appeared to influence the work reported in this paper.

Acknowledgements

This research is gratefully supported by the Engineering and Physical Sciences Research Council (EPSRC) through their funding of the STREAM Industrial Doctorate Centre (EP/ G037094/1) and from the project sponsor Anglian Water. Supplementary information and data sets are available: DOI: 10.17862/cranfield.rd.19614633.

Appendix A. Supplementary data

Supplementary data to this article can be found online at https://doi.org/10.1016/j.jwpe.2025.106963.

Data availability

data sets are available: DOI: 10.17862/cranfield.rd.19614633.

References

[1] I. Levitsky, D. Tavor, V. Gitis, Micro and nanobubbles in water and wastewater treatment: a state-of-the-art review, Journal of Water Process Engineering 47 (2022) 102688, https://doi.org/10.1016/j.jwpe.2022.102688.
[2] A. John, A. Brookes, I. Carra, B. Jefferson, P. Jarvis, Microbubbles and their application to ozonation in water treatment: a critical review exploring their benefit and future application, Crit. Rev. Environ. Sci. Technol. 52 (9) (2022) 1561–1603, https://doi.org/10.1080/10643389.2020.1860406.
[3] B. Singh, N. Shukla, C. Cho, B. Kim, M. Park, K. Kim, Effect and application of micro- and nanobubbles in water purification, Toxicol. Environ. Heal. Sci. 13 (1) (2021) 9–16, https://doi.org/10.1007/s13530-021-00081-x.
[4] S. Movahed, A. Sarmah, Global trends and characteristics of nano- and microbubbles research in environmental engineering over the past two decades: a scientometric analysis, Sci. Total Environ. 785 (2021) 147362, https://doi.org/10.1016/j.scitotenv.2021.147362.
[5] T. Temesgen, T. Bui, M. Han, T. Kim, H. Park, Micro and nanobubble technologies as a new horizon for water-treatment techniques: a review, Adv. Colloid Interf. Sci. 246 (2017) 40–51, https://doi.org/10.1016/j.cis.2017.06.011.
[6] G. Baquero-Rodríguez, J. Lara-Borrero, D. Nolasco, D. Rosso, A critical review of the factors affecting modeling oxygen transfer by fine-pore diffusers in activated sludge, Water Environ. Res. 90 (5) (2018) 431–441, https://doi.org/10.2175/106143017X15131012152988.
[7] J. Behnisch, A. Ganzauge, S. Sander, M. Herrling, M. Wagner, Improving aeration systems in saline water: measurement of local bubble size and volumetric mass transfer coefficient of conventional membrane diffusers, Water Sci. Technol. 78 (4) (2018) 860–867, https://doi.org/10.2166/wst.2021.185.
[8] M. Garrido-Baserba, P. Asvapathanagul, H. Park, T. Kim, G. Baquero-Rodriguez, B. Olson, D. Rosso, Impact of fouling on the decline of aeration efficiency under different operational conditions at WRRFs, Sci. Total Environ. 639 (2018) 248–257, https://doi.org/10.1016/j.scitotenv.2018.05.036.
[9] M. Terashima, M. So, R. Goel, H. Yasui, Determination of diffuser bubble size in computational fluid dynamics models to predict oxygen transfer in spiral roll aeration tanks, Journal of Water Process Engineering 12 (2016) 120–126, https://doi.org/10.1016/j.jwpe.2016.07.001.
[10] Y. Shangguan, S. Yu, C. Gong, Y. Wang, W. Yang, L. Hou, A review of microbubble and its applications in ozonation, IOP Conference Series: Earth and Environmental Science 128 (2018) 012149, https://doi.org/10.1088/1755-1315/128/1/012149.
[11] R. Parmar, S. Majumder, Microbubble generation and microbubble-aided transport process intensification—a state-of-the-art report, Chem. Eng. Process. Process Intensif. 64 (2013) 79–97, https://doi.org/10.1016/j.cep.2012.12.002.

[12] N. Suwartha, D. Syamzida, C. Priadi, S. Moersidik, F. Ali, Effect of size variation on microbubble mass transfer coefficient in flotation and aeration processes, Heliyon 6 (4) (2020) e03748, https://doi.org/10.1016/j.heliyon.2020.e03748.
[13] A. John, I. Carra, B. Jefferson, L. Bertolaso, A. Brookes, P. Jarvis, Enhancement of ozonation using microbubbles – micropollutant removal, mass transfer and bromate formation, Chem. Eng. Sci. 283 (2024) 119369, https://doi.org/10.1016/j.ces.2023.119369.
[14] A. Atkinson, O. Apul, O. Schneider, S. Garcia-Segura, P. Westerhoff, Nanobubble technologies offer opportunities to improve water treatment, Acc. Chem. Res. 52 (5) (2019) 1196–1205, https://doi.org/10.1021/acs.accounts.8b00606.
[15] M. Abbasian-arani, M. Hatamipour, A. Rahimi, Experimental determination of gas holdup and volumetric mass transfer coefficient in a jet bubbling reactor, Chin. J. Chem. Eng. 34 (2021) 61–67, https://doi.org/10.1016/j.cjche.2020.07.051.
[16] Lyu, T., Wu, S., Mortimer, R. and Pan, G., 2019. Nanobubble Technology in Environmental Engineering: Revolutionization potential and challenges. *Environmental Science & Technology*, 53(13), pp.7175–7176. doi:https://doi.org/10.1021/acs.est.9b02821.
[17] M. Farid, P. Choi, J. Kharraz, J. Lao, S. St-Hilaire, Y. Ruan, P. Lam, A. An, Hybrid nanobubble-forward osmosis system for aquaculture wastewater treatment and reuse, Chem. Eng. J. 435 (2022) 135164, https://doi.org/10.1016/j.cej.2022.135164.
[18] K. Ulatowski, M. Sidorski, P. Sobieszuk, Oil-contaminated surface cleaning using oxygen and nitrogen Nanobubbles, J. Phys. Conf. Ser. 1681 (1) (2020) 012017, https://doi.org/10.1088/1742-6596/1681/1/012017.
[19] Y. Tang, M. Zhang, J. Zhang, T. Lyu, M. Cooper, G. Pan, Reducing arsenic toxicity using the interfacial oxygen nanobubble technology for sediment remediation, Water Res. 205 (2021) 117657, https://doi.org/10.1016/j.watres.2021.117657.
[20] H. Zhang, L. Jiawei, Y. Shanshan, Z. Xiyang, F. Rongxin, H. Xinyu, L. Ji, High efficiently utilizing micro-nano ozone bubbles to enhance electro-peroxide process for rapid removal of trace pharmaceutical contaminants from hospital wastewater, Water Res. 259 (2024) 121896, https://doi.org/10.1016/j.electacta.2022.141708.
[21] A. Sharifi, S.F. Saghravani, K. Ghasemipanah, B. Daharazma, B. Rasekh, Evaluation of the performance of air micro-nano bubbles for cleaning in place to reduce the reverse osmosis membrane clogging, Desalin. Water Treat. 320 (2024) 100599, https://doi.org/10.1016/j.dwt.2024.100599.
[22] D. Rak, M. Ovadová, M. Sedlák, (non)existence of bulk Nanobubbles: the role of ultrasonic cavitation and organic solutes in water, The Journal of Physical Chemistry Letters 10 (15) (2019) 4215–4221, https://doi.org/10.1021/acs.jpclett.9b01402.
[23] Patel, A.K., Singhania, R.R., Chen, C-W., Tseng, Y-S., Kuo, C-H., Wu, C-H. and Dong, C.D., 2021. Advances in micro- and nano bubbles technology for application in biochemical processes. Environ. Technol. Innov., 23, p.101729. doi:https://doi.org/10.1016/j.eti.2021.101729.
[24] A. Jadhav, M. Barigou, Bulk Nanobubbles or not Nanobubbles: that is the question, Langmuir 36 (7) (2020) 1699–1708, https://doi.org/10.1021/acs.langmuir.9b03532.
[25] P. Epstein, M. Plesset, On the stability of gas bubbles in liquid-gas solutions, J. Chem. Phys. 18 (11) (1950) 1505–1509, https://doi.org/10.1007/BF0038594.
[26] M. Alheshibri, V. Craig, Differentiating between nanoparticles and Nanobubbles by evaluation of the compressibility and density of nanoparticles, J. Phys. Chem. C 122 (38) (2018) 21998–22007, https://doi.org/10.1021/acs.jpcc.8b07174.
[27] M. Alheshibri, V. Craig, Generation of nanoparticles upon mixing ethanol and water; Nanobubbles or not? J. Colloid Interface Sci. 542 (2019) 136–143, https://doi.org/10.1016/j.jcis.2019.01.134.
[28] M. Alheshibri, M. Jehannin, V. Coleman, V. Craig, Does gas supersaturation by a chemical reaction produce bulk nanobubbles? J. Colloid Interface Sci. 554 (2019) 388–395, https://doi.org/10.1016/j.jcis.2019.07.016.
[29] V. Leroy, T. Norisuye, Investigating the existence of bulk Nanobubbles with ultrasound, ChemPhysChem 17 (18) (2016) 2787–2790, https://doi.org/10.1002/cphc.201600576.
[30] M. Sedlák, D. Rak, Large-scale Inhomogeneities in solutions of low molar mass compounds and mixtures of liquids: supramolecular structures or Nanobubbles? J. Phys. Chem. B 117 (8) (2013) 2495–2504, https://doi.org/10.1021/jp4002093.
[31] A. Häbich, W. Ducker, D. Dunstan, X. Zhang, Do stable Nanobubbles exist in mixtures of organic solvents and water? J. Phys. Chem. B 114 (20) (2010) 6962–6967, https://doi.org/10.1021/jp911868j.
[32] A. Jadhav, M. Barigou, Response to “comment on bulk Nanobubbles or not Nanobubbles: that is the question”, Langmuir 37 (1) (2021) 596–601, https://doi.org/10.1021/acs.langmuir.0c03165.
[33] Z. Fang, X. Wang, L. Zhou, L. Zhang, J. Hu, Formation and stability of bulk Nanobubbles by vibration, Langmuir 36 (9) (2020) 2264–2270, https://doi.org/10.1021/acs.langmuir.0c00036.
[34] W. Kanematsu, T. Tuziuti, K. Yasui, The influence of storage conditions and container materials on the long term stability of bulk nanobubbles — consideration from a perspective of interactions between bubbles and surroundings, Chem. Eng. Sci. 219 (2020) 115594, https://doi.org/10.1016/j.ces.2020.115594.
[35] G. Manning, On the thermodynamic stability of bubbles, immiscible droplets, and cavities, Phys. Chem. Chem. Phys. 22 (31) (2020) 17523–17531, https://doi.org/10.1039/D0CP02517H.
[36] H. Zhang, Z. Guo, X. Zhang, Surface enrichment of ions leads to the stability of bulk nanobubbles, Soft Matter 16 (23) (2020) 5470–5477, https://doi.org/10.1039/D0SM00116C.
[37] N. Nirmalkar, A. Pacek, M. Barigou, Bulk Nanobubbles from acoustically Cavitated aqueous organic solvent mixtures, Langmuir 35 (6) (2019) 2188–2195, https://doi.org/10.1021/acs.langmuir.8b03113.
[38] Eklund, F., Alheshibri, M. and Swenson, J., 2021. Differentiating bulk nanobubbles from nanodroplets and nanoparticles. *Current Opinion in Colloid & Interface Science*, 53, p.101427. doi:https://doi.org/10.1016/j.cocis.2021.101427.
[39] M. Abbasian-arani, M. Hatamipour, A. Rahimi, Experimental determination of gas holdup and volumetric mass transfer coefficient in a jet bubbling reactor, Chin. J. Chem. Eng. 34 (2021) 61–67, https://doi.org/10.1016/j.cjche.2020.07.051.
[40] Z. Usfoor, K. Kaufmann, A. Rakib, R. Hergenröder, V. Shpacovitch, Features of sizing and enumeration of silica and polystyrene nanoparticles by nanoparticle tracking analysis (NTA), Sensors 20 (22) (2020) 6611, https://doi.org/10.3390/s20226611.
[41] D. Bachurski, M. Schuldner, P. Nguyen, A. Malz, K. Reiners, P. Grenzi, F. Babatz, A. Schauss, H. Hansen, M. Hallek, E. Pogge von Strandmann, Extracellular vesicle measurements with nanoparticle tracking analysis – An accuracy and repeatability comparison between NanoSight NS300 and ZetaView, Journal of Extracellular Vesicles 8 (1) (2019) 1596016, https://doi.org/10.1080/20013078.2019.1596016.
[42] S. Zhou, S. Nazari, A. Hassanzadeh, X. Bu, C. Ni, Y. Peng, G. Xie, Y. He, The effect of preparation time and aeration rate on the properties of bulk micro-nanobubble water using hydrodynamic cavitation, Ultrason. Sonochem. 84 (2022) p105965, https://doi.org/10.1016/j.ultsonch.2022.105965.
[43] A. John, I. Carra, B. Jefferson, M. Jodkowska, A. Brookes, P. Jarvis, Are microbubbles magic or just small? A direct comparison of hydroxyl radical generation between microbubble and conventional bubble ozonation under typical operational conditions, Chem. Eng. J. (2022) 134854, https://doi.org/10.1016/j.cej.2022.134854.
[44] J. Zhang, G. Huang, C. Liu, R. Zhang, X. Chen, L. Zhang, Synergistic effect of microbubbles and activated carbon on the ozonation treatment of synthetic dyeing wastewater, Sep. Purif. Technol. 201 (2018) 10–18, https://doi.org/10.1016/j.seppur.2018.02.003.
[45] T. Takemura, H. Shoichiro, S. Minoru, S. Kenichiro, O. Koichi, Migration behaviour and lifetime of CO2 micro-nano bubbles in shallow aquifer, International Journal of Greenhouse Gas Control 137 (2024) 104207, https://doi.org/10.1016/j/ijggc.2024.104207.
[46] W. Sun, L. Guicai, R. Xiao, L. Chao, Q. Liping, Z. Shoubin, X. Kang, Hydroxyl radical generated by micro-nano bubbles and its application in water treatment, Proc. SPIE-Int. Soc. Opt. Eng. 12255 (2022) 122552V, https://doi.org/10.1117/12.2638618.
[47] K. Yasui, T. Tuziuti, W. Kanematsu, K. Kato, Dynamic equilibrium model for a bulk Nanobubble and a microbubble partly covered with hydrophobic material, Langmuir 32 (43) (2016) 11101–11110, https://doi.org/10.1021/acs.langmuir.5b04703.
[48] Mitra, S., Johnston, R., Scott, K., Lin, R., Wyatt, F., Coffey, B. and Rakness, K., 2017. Ozone plant operations under drought conditions. *Ozone: Science & Engineering*, 39(3), pp.202–208. doi:https://doi.org/10.1080/01919512.2017.1289467.
[49] M. Kim, M. Han, T. Kim, J. Lee, D. Kwak, Effect of nanobubbles for improvement of water quality in freshwater: flotation model simulation, Sep. Purif. Technol. 241 (2020) 116731, https://doi.org/10.1016/j.seppur.2020.116731.
[50] G. Vezzu, J. Lopez, A. Freilich, K. Becker, Optimization of large-scale ozone generators, IEEE Trans. Plasma Sci. 37 (6) (2009) 890–896, https://doi.org/10.1109/TPS.2009.2015452.
[51] F. Soltermann, C. Abegglen, M. Tschui, S. Stahel, U. von Gunten, Options and limitations for bromate control during ozonation of wastewater, Water Res. 116 (2017) 76–85, https://doi.org/10.1016/j.watres.2017.02.026.
[52] H.N.P. Dayarathne, S. Jeong, A. Jang, Chemical-free inhibition method for seawater reverse osmosis membrane process: air micro-nano bubbles, Desalination 461 (2019) 1–9, https://doi.org/10.1016/j.desal.2019.03.008.

Understanding the difference between the nano and micro bubble size distributions generated by a regenerative turbine microbubble generator using ozone

John, Alexander

2025-02-01

John A, Brookes A, Carra I, et al., (2025) Understanding the difference between the nano and micro bubble size distributions generated by a regenerative turbine microbubble generator using ozone. Journal of Water Process Engineering, Volume 70, February 2025, Article number 106963
https://doi.org/10.1016/j.jwpe.2025.106963